

Rapidly separable bubble microneedle patch for effective local anesthesia

Yuan Yang^{1,2,§}, Huaqing Chu^{3,§}, Yan Zhang^{4,§}, Lingling Xu⁵, Ruizeng Luo¹, Hui Zheng³ (✉), Tailang Yin⁶ (✉), and Zhou Li^{1,2,7,8} (✉)

¹ CAS Center for Excellence in Nanoscience Beijing Key Laboratory of Micro-nano Energy and Sensor, Beijing Institute of Nanoenergy and Nanosystems, Chinese Academy of Sciences, Beijing 101400, China

² School of Nanoscience and Technology, University of Chinese Academy of Sciences, Beijing 100049, China

³ Department of Anesthesiology, National Cancer Center/National Clinical Research Center for Cancer/Cancer Hospital, Chinese Academy of Medical Sciences and Peking Union Medical College, Beijing 100021, China

⁴ Department of Clinical Laboratory, Renmin Hospital of Wuhan University, Wuhan 430060, China

⁵ CAS Key Laboratory for Biomedical Effects of Nanomaterials and Nanosafety and CAS Center for Excellence in Nanoscience, National Center for Nanoscience and Technology, Beijing 100190, China

⁶ Reproductive Medicine Center, Renmin Hospital of Wuhan University, Wuhan 430060, China

⁷ School of Chemistry and Chemical Engineering, Center on Nanoenergy Research, Guangxi University, Nanning 530004, China

⁸ Institute for Stem Cell and Regeneration, Chinese Academy of Sciences, Beijing 100101, China

[§] Yuan Yang, Huaqing Chu, and Yan Zhang contributed equally to this work.

© Tsinghua University Press 2022

Received: 15 April 2022 / Revised: 4 May 2022 / Accepted: 6 May 2022

ABSTRACT

In cutaneous cosmetology surgery, local injection or coated anesthetics are generally used to provide analgesia at the treatment site to achieve painless operation. Due to the barrier of corneum, topical cream may cause uncertain dosage and delayed analgesia. Local injection has problems such as pain, infection, and misoperation. Therefore, it is necessary to develop a painless and rapid administration method for local anesthesia. Here, a lidocaine/hyaluronic acid bubble microneedle patch (Lido/HA bMNP) was prepared for rapid drug delivery and efficient analgesia. The bubble structure between microneedles (MNs) and the backing layer allowed the MNs to efficiently penetrate into the skin and remove from the backing layer under shear force to rapidly complete the administration. Drugs were quickly released with the dissolution of HA within 15 s, which immediately played an analgesic effect and lasted for 1 h. Lido/HA bMNP could deliver precise doses to the skin in an extremely short time, which had the advantages of convenient operation, high biosafety, rapid onset of analgesia, and reasonable pain relief time. This patch provided an alternative way for local anesthesia and it was a promising transdermal drug delivery method for the realization of high quality and efficiency “painless medical beauty”.

KEYWORDS

separable bubble microneedle patch, hyaluronic acid, rapid drug delivery, local anesthesia, cutaneous cosmetology surgery

1 Introduction

With the continuous progress of medical technology and individual pursuit of beauty in recent years, the medical cosmetic industry is gradually growing, especially for light medical beauty projects. Most aesthetic surgery has a certain degree of pain, so adequate analgesia is required during surgery [1, 2]. Some dermatological surgeries and medical beauty treatment in plastic surgery, including superficial skin surgeries (e.g., nevus removal, vegetations excision, and superficial skin tumor resection) and minimally invasive cosmetic procedures (e.g., skin laser treatment), generally have a short operation time, small and superficial wound, and only local anesthesia is needed to meet the needs of surgical analgesia. Local anesthesia is relatively safer due to low physical stress, less drug dosage, and fast recovery [3]. Injectable anesthesia and spray or cream application are common

forms of anesthetic administration for local analgesia [4, 5]. However, injection anesthesia requires high operation requirements for injection personnel and patients have lower compliance [6]. Systemic toxicity may occur with excessive administration or with accidental intravascular injection and can result in loss of consciousness, seizures, cardiac rhythm disturbances, and cardiovascular collapse [7, 8]. Topical anesthetics usually have a slower onset of action and require longer waiting times due to the barrier of the stratum corneum [9]. At the same time, considering individual differences, insufficient anesthesia may occur and eventually affect the operation process. Therefore, it is necessary to develop a painless and rapid transdermal drug delivery method for the delivery of local anesthetics.

As a minimally invasive device, microneedles (MNs) can

Address correspondence to Hui Zheng, zhenghui@cicams.ac.cn; Tailang Yin, reproductive@whu.edu.cn; Zhou Li, zli@binn.cas.cn

painlessly penetrate the stratum corneum and form microchannels into the epidermis or dermis [10–12]. As a result, drug molecules can bypass the skin barrier and diffuse into the subcutaneous tissue [13, 14]. Apart from the painless and mini-invasive administration [15–17], the advantages of MNs for transdermal delivery include avoiding emotional trauma and injection risk [18–20], elevating the efficiency of drug delivery [21], as well as decreasing the transportation and preservation of pharmaceuticals and reducing medical waste [22, 23]. MNs provide appropriate administration for local analgesia [24, 25]. The current MNs for analgesia mainly include solid MNs, coated MNs, and dissolving MNs [26]. Solid MNs are usually used for skin pretreatment, which is difficult to precisely control the dosage [27, 28]. Coated MNs could relatively accurately control the dosage in the process of percutaneous administration, but it is difficult to achieve an effective dose on MN surface [29]. Dissolving MNs are made of water soluble materials as the matrix [30]. Generally, drug loading could be improved by loading drugs on the needle [31, 32]. However, rapid and accurate drug delivery remains a challenge due to the difficulty of ensuring complete insertion and efficient dissolution of the MNs. In addition, since the microneedle patch (MNP) is easily detached from the skin, long-term compression is required to complete the administration. Dissolving MNs with bubbles provide an opportunity to shorten administration times, which could rapidly separate the patch backing layer from the needle [33–35]. Nevertheless, improving the drug loading and separation rate of bubble MNs is another key challenge.

Given these objectives and challenges, we developed a lidocaine/hyaluronic acid bubble microneedle patch (Lido/HA bMNP) for local anesthesia, which was prepared with two different materials, and the needle and the backing layer were made of HA and polyvinyl alcohol (PVA), respectively. Taking advantage of different water absorption properties of HA and

PVA, when Lido/HA bMNP was applied to the skin, the HA MNs could be easily separated from the backing to achieve rapid drug administration. The drug loading capacity of Lido/HA bMNP was improved by the method of drug loading on the tip and matrix material, and repeatedly coating the drug solution and vacuuming. Lido/HA bMNP could contain 107 μg Lido and release it within 15 s with accurate drug loading and rapid drug release rate. In cell experiments, it was demonstrated that Lido/HA bMNP has high biosafety for local analgesia. Analgesic effect on the plantar incision model (PIM) showed Lido/HA bMNP could rapidly relieve pain and sustain for 1 h, which satisfied the requirements of minimally invasive cosmetic surgery. The patch has the advantages of low preparation cost, convenient operation, rapid onset of analgesia, and a reasonable duration of analgesia.

2 Results and discussion

2.1 Design and fabrication of Lido/HA bMNP

In this work, a Lido/HA bMNP was designed for rapid delivery of anesthetics. HA was used to prepare the dissolving MNs, which is a natural hydrophilic molecule that absorbs and retains moisture, making skin soft, smooth, and elastic, thus preventing skin aging or wrinkles [36, 37]. The patch backing was fabricated using 35% PVA, which is a safe and water-soluble material. To facilitate the rapid drug administration, a bubble was created between MNs and the patch backing. The process of Lido/HA bMNP transdermal drug delivery is shown in Fig. 1(a). After the MN penetrated the skin vertically, the drug-loaded MN body was dissolved and implanted into the skin with the action of a weak shear force due to the presence of bubbles structure and different water absorption properties of HA and PVA. Then, Lido was quickly released with the dissolution of HA MNs. As illustrated in Fig. 1(b), Lido/HA bMNP would hold promise for topical analgesia in minimally invasive cosmetic procedures such as

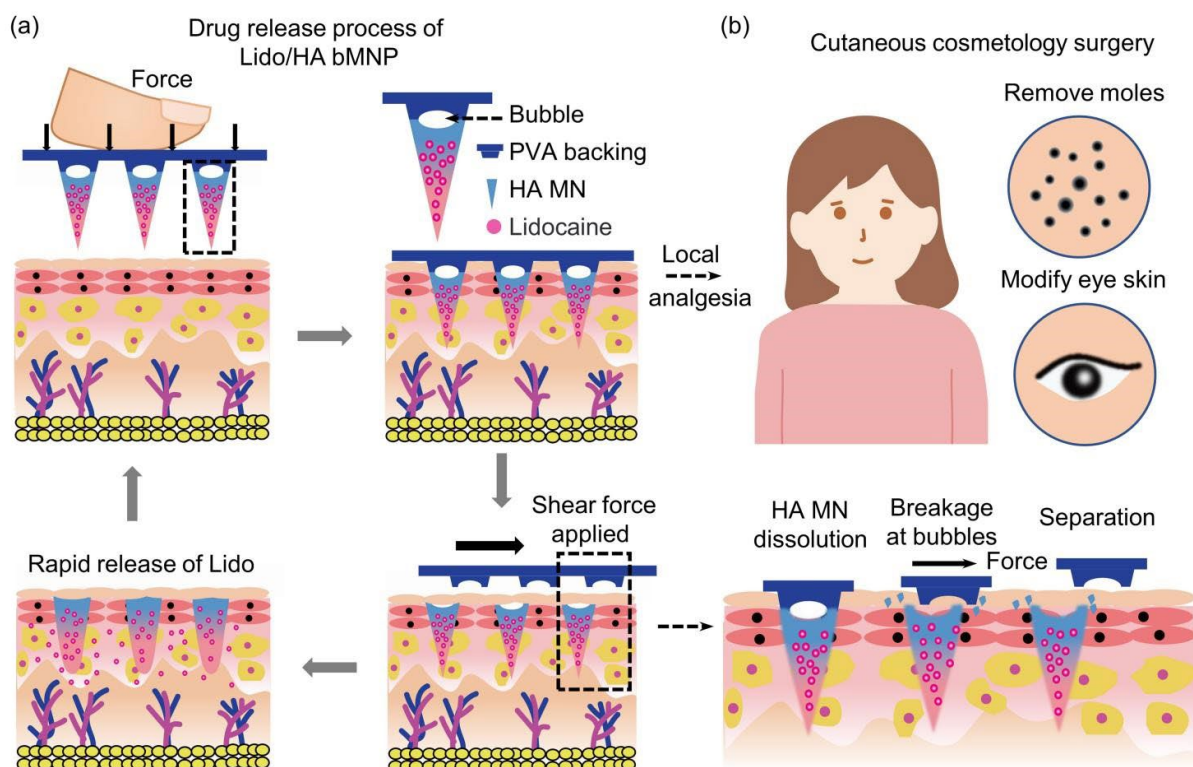


Figure 1 Design of Lido/HA bMNP. (a) Right and inset: schematic of the design of Lido/HA bMNP containing a bubble for rapid separation of the MNs from the backing layer. Left: the process of Lido/HA bMNP application to the skin with vertical force and MN delivery into the skin using shear force for the rapid release of encapsulated Lido. (b) Lido/HA bMNP for analgesia in medical cosmetic surgery such as removing moles and modifying eye skin.

removal of superficial moles or tumors and modification of ocular skin.

As shown in Fig. 2(a), Lido/HA bMNP was fabricated by using a mold casting method. The Lido solution was filled in the cavity under vacuum, dried and collected at the tip of the cavity. The drug loading of MN was enhanced by repeatedly adding the Lido solution to the polydimethylsiloxane (PDMS) mold. Next, HA solution mixed with Lido was cast onto the mold to fill the cavities under vacuum. Following the excess solution was removed, a

sunken structure was formed in the cavity under vacuum due to the insufficient polymer matrix. The aqueous PVA backing solution was applied to the mold, and a bubble solidified in the MNs after drying. It can be seen from Figs. 2(b)–2(d) that Lido/HA bMNP was designed as 10×10 MN array on a $7 \text{ mm} \times 7 \text{ mm}$ substrate, with a needle body height of $700 \mu\text{m}$, a bottom diameter of $300 \mu\text{m}$, and a needle spacing of $500 \mu\text{m}$. The position of the bubble could be controlled by adjusting the vacuuming time of the Lido/HA matrix material. As shown in Fig. 2(e), when the

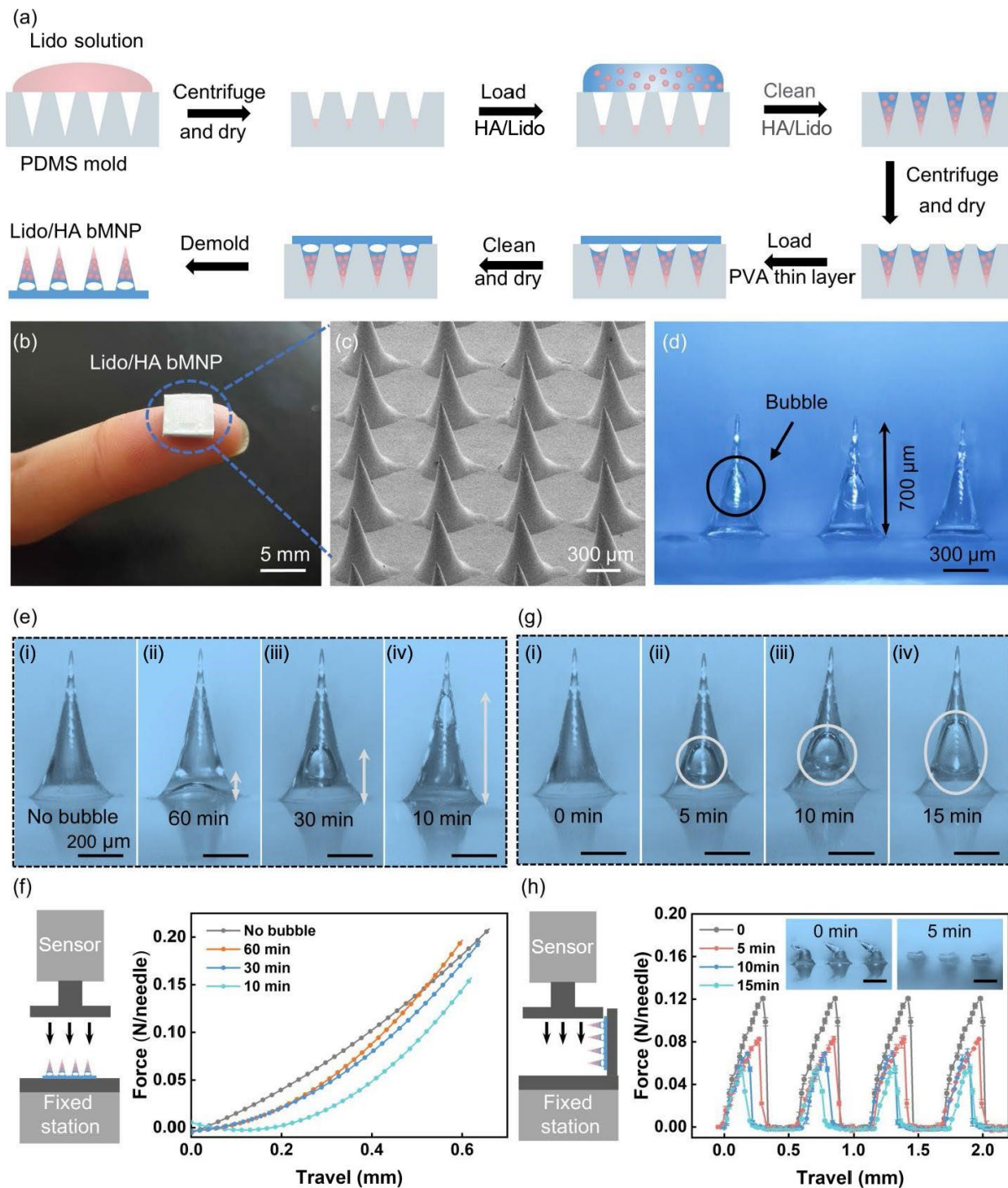


Figure 2 Characterization of Lido/HA bMNP. (a) Schematic of the fabrication process of Lido/HA bMNP. (b) Lido/HA bMNP shown resting on a finger. (c) SEM image of Lido/HA bMNP with an array of MNs. (d) Representative bright-field microscopy images of MNs containing bubbles. The black circle identifying bubble structures. (e) Representative bright field microscopy images of Lido/HA MNP (no bubble) and Lido/HA bMNP with bubbles in different positions of needle, fabricated using different vacuuming time of Lido/HA matrix material, 10, 30, and 60 min. (f) Typical force displacement curve of Lido/HA MNP and Lido/HA bMNP in different positions. (g) Representative bright field microscopy images of Lido/HA MNP (0 min) and Lido/HA bMNP with bubbles of different sizes generated by forming the sunken structure of different depths with different vacuum times of 5, 10, and 15 min. (h) Horizontal force displacement curve of Lido/HA MNP and Lido/HA bMNP with bubbles of different sizes. (Inset) The representative bright-field microscopy images of MNs without bubble (left) and bubble MNs (right) after the application of shear force. Scale bar, $300 \mu\text{m}$.

vacuuming time were 10, 30, and 60 min, the corresponding heights of the bubbles were 500, 300, and 100 μm , respectively. This was because the longer the vacuuming time, the more Lido/HA matrix material was filled into the PDMS cavity, and the position of the subsequently formed bubbles was closer to the backing layer. The force and displacement curves were presented in Fig. 2(f), the slope of the Lido/HA bMNP gradually became larger and the mechanical properties of MN gradually became better as bubbles position approached the base. Therefore, the vacuuming time of the Lido/HA matrix was set to 60 min to prepare Lido/HA bMNP. At the same time, as shown in Fig. 2(g), the bubble size was controlled by adjusting the vacuuming time to form the sunken structure [38], as the increased time of the vacuuming promoted deeper depressions and bigger bubble in MN. The size of the bubbles affected the mechanical properties of the MNs [39]. As seen from Fig. 2(h), bMNP was easily broken under the shear force of 0.08 N/needle, while MNP without bubbles required a significantly larger shear of 0.12 N/needle to bend and deform, indicating that due to the existence of the bubble structure, Lido/HA bMNs could be easily separated from the backing layer and implanted in the skin tissue under weak shear force. However, the mechanical properties of the MN deteriorate with the increase of the bubble volume. Hence, the vacuuming time of the HA solution was 60 min, and the bubble formation time was 5 min, which were the optimal conditions for the preparation of MNs.

2.2 Drug delivery *in vitro* and *in vivo*

To determine whether the bMNP could rapidly release the drug when applied to the skin, as shown in Figs. 3(a) and 3(b), we pressed the bMNP into the pig skin. MNs are loaded with rhodamine B dye instead of Lido for visualization. Figure 3(c) presents MNs penetrated the skin, detached from the patch backing, and embedded in the skin after applying a gentle shear, and Fig. 3(d) shows that there was little residual red dye in the MNs, proving the efficient drug delivery of the MNs into the skin.

The content of Lido encapsulated in MNs determines its analgesic effect. The drug loading of MNs mainly depended on the concentration of Lido solution and the content of Lido/HA matrix material during the preparation process. However, the high content of Lido in the needle may affect the mechanical properties of the microneedle. The skin piercing ability is the premise of drug-loaded MNs for transdermal drug delivery. Stronger polymer MNs facilitate transdermal drug delivery at stiffer body tissue sites, while weaker mechanical behavior limits the application of MNs [40]. The optimal formulation of Lido/HA bMNP was determined by analyzing the mechanical properties and penetration capabilities of MNs, which were completed by applying axial compressive load to the MNs and inserting the prepared MNs into parafilm and animal skins. The drug loading of Lido/HA bMNP was investigated in 0.01 mol/L phosphate buffer solution (PBS), and the MNs were completely dissolved within 15 s. As seen from Fig. 3(e), the Lido loadings in Lido/HA bMNP prepared with Lido concentrations of 1, 5, 10, and 20 mg/L were 0.01 ± 0.009 , 0.08 ± 0.008 , 0.11 ± 0.009 , and 0.24 ± 0.001 $\mu\text{g}/\text{needle}$, respectively. The results showed that the drug loading of the MNs increased with the concentration of Lido solution. However, Fig. 3(f) shows that the mechanical properties of the MNs dropped sharply when the Lido concentration was 20 mg/mL, which was attributed to the accumulation of a large amount of Lido powder on the needle tip and the lack of HA matrix material. Therefore, the Lido concentration of 10 mg/mL was the most suitable parameter to be used to prepare the MNs. In order to further improve the drug loading of MNs, HA matrix material mixed with Lido was used to prepare MNs. As shown in

Fig. 3(g), the higher the mixed Lido content in the HA matrix material, the higher the drug loading of the MNs. The Lido loadings in Lido/HA bMNP with Lido contents in HA matrix material of 10%, 20%, 30%, 40%, and 50% were 0.58 ± 0.016 , 1.07 ± 0.046 , 1.74 ± 0.052 , 2.50 ± 0.023 , and 3.18 ± 0.012 $\mu\text{g}/\text{needle}$, respectively. However, Fig. 3(h) presents that the mechanical properties of the MNs also gradually deteriorate when the content of Lido increases. The penetration ability of the MNs was evaluated by penetrating the MNs into the multilayer parafilm that mimicking skin tissue, and the penetration depth of the prepared Lido/HA bMNP could be evaluated from the pores generated in each layer. The experimental results were shown in Fig. 3(i), with the increase of Lido content in the HA matrix material, the penetration ability of the MNs gradually weakened. Most importantly, as shown in Fig. 3(j), when Lido/HA bMNP was applied to the skin of mice, the needles of Lido/HA bMNP with the Lido concentration of more than 20% cannot fully penetrate the skin. Considering the drug loading and mechanical properties of Lido/HA bMNP, Lido concentration of 10 mg/mL and Lido content of 20% in HA matrix were the optimal formulations for the preparation of MNs.

To visualize the drug release process *in vivo*, rhodamine B instead of Lido was encapsulated in bMNP. The patch was manually applied to the mouse skin and gently sheared, the MNs penetrated the skin, detached from the backing layer, and fully embedded in the skin. In Figs. 3(k) and 3(l), *in vivo* imaging and fluorescence intensity at the administration site showed that more drugs were rapidly released from the MNs and further diffused into the deep skin tissue compared with the same drug-loaded HA hydrogel patch. It indicated that bMNP could rapidly separate from the backing and quickly release drugs *in vivo*.

2.3 Biosafety assessment

To achieve the effect of local analgesia, Lido acts on the tissue of the surgical area to block peripheral nerve endings. In this process, there is a chance that some Lido could be absorbed into the blood. Excessive intake of lidocaine the bloodstream may cause mild headache and tinnitus, visual disturbances, muscle twitching, convulsions, loss of consciousness, and finally coma. Cardiovascular depression and respiratory arrest could occur at very high plasma concentrations. Lido toxicity was evaluated in L929 fibroblast cells [41, 42]. As shown in Figs. 4(a) and 4(b), the images of fluorescence staining showed that L929 cells grew slowly and died easily when incubated with 400 and 800 $\mu\text{g}/\text{mL}$ Lido. When the Lido concentration was 200, 400, and 800 $\mu\text{g}/\text{mL}$, the cell viability was 86.65%, 74.15%, and 62.81%, respectively. With the increase of Lido concentration, the cell viability significantly decreased, indicating that excessive Lido had certain toxic and side effects on the cells. Therefore, it is critical to strictly control the dose of Lido during surgery. Interestingly, Lido/HA bMNP can pierce the skin stratum corneum and transport the accurate dose of Lido to the skin tissue, and it would not touch the skin blood vessels, avoiding excessive Lido into the blood to cause a certain toxic side reaction. Furthermore, we further evaluated the material toxicity of the MNs. As shown in Figs. 4(c)–4(f), the cell viabilities of HA, PVA, and Lido/HA bMNs were all above 80%, and the cell viability was almost unchanged with the increase of material concentration. These results fully demonstrated the high biosafety of Lido/HA bMNP for local analgesia.

2.4 Lido/HA MNs analgesia *in vivo*

As illustrated in Fig. 5(a), we selected the classic acute postoperative pain, Brennan's plantar incision model to evaluate the local analgesic effect of HA soluble MNs containing Lido [43]. Figure 5(b) showed that the Brennan's plantar incision model was

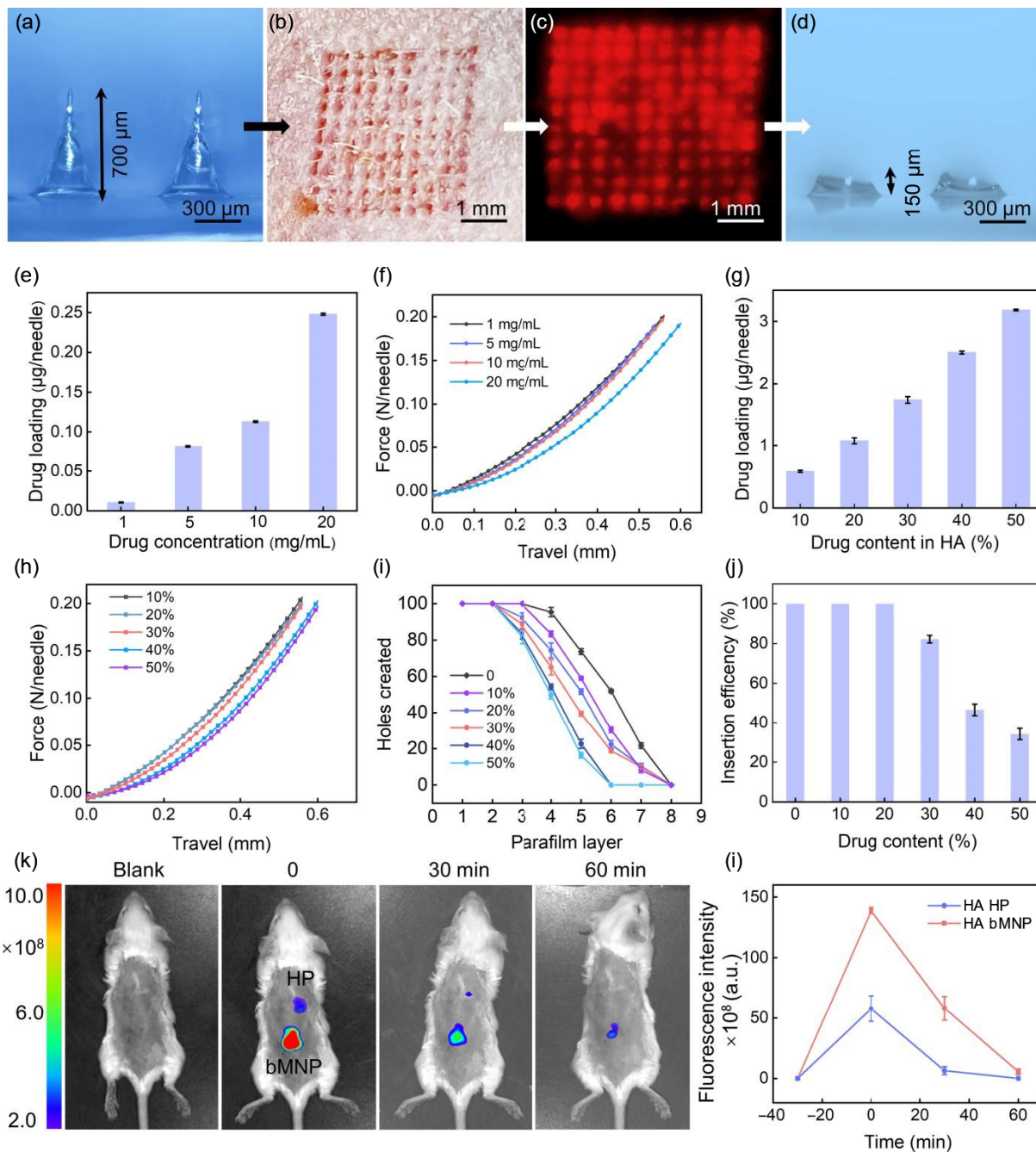


Figure 3 Drug delivery *in vitro* and *in vivo*. (a) Representative bright-field microscopy images of Lido/HA bMNP. (b) Representative bright-field and (c) fluorescence microscopy images of porcine skin after MNP insertion and drug delivery *in vitro*. (d) Representative bright-field microscopy image of MNP backing layer after application to porcine skin *in vitro*, showing detachment of the MNs from the backing layer and release of drugs. (e) Drug loading of Lido/HA bMNP fabricated with different drug concentrations, 1, 5, 10, and 20 mg/mL. (f) Typical force-displacement curve of Lido/HA bMNP fabricated with different drug concentration. (g) Drug loading of Lido/HA bMNP fabricated with HA matrix materials containing different drug contents of 10%, 20%, 30%, 40% and 50%. (h) Typical force-displacement curves of Lido/HA bMNP fabricated with different drug content in HA matrix material. (i) Holes created in each parafilm layer after insertion of Lido/HA bMNP using constant 5 N. (j) Skin insertion efficiency of Lido/HA bMNP. (k) and (l) Fluorescence images and fluorescence intensity of skin administration area by Lido/HA bMNP and Lido/HA HP at different times.

constructed by longitudinally incising the skin and fascia of the heel to expose the toe muscles, and then longitudinally splitting flexor digitorum brevis muscle. All rats were allowed to acclimatize in the laboratory for two days; then baseline measurements were completed before modeling. Rats were allowed to recover for one day post-surgery, and the postoperative mechanical paw withdrawal threshold (PWT) was tested on the first day after operation. The mechanical threshold of all PIM rats decreased significantly to $39.34\% \pm 6.0\%$ of pre-PIM baseline, confirming successful modeling. Then PIM rats in each group were treated with Lido/HA bMNP (107 μg Lido/patch), Lido hydrogel patch (Lido HP, 107 μg Lido/patch), HA bMNP without

drugs, and no treatment as the black control group, respectively. As shown in Fig. 5(c), the Lido/HA bMNP was applied vertically to the skin on both sides of the wound, and the backing layer was removed using a transverse shear force. The behavioral tests were performed at scheduled time points (15, 30, 45, 60, 75, and 90 min) post administration. In Figs. 5(d)–5(f), the mechanical PTW showed significant difference across all time points of post-operation compared to the baseline. There was no significant difference of PWT between HA bMNP group and blank group. The threshold of the Lido HP group was slightly improved at 15, 30, 45, 60, and 75 min post administration compared to blank group, and Lido HP produced only a small analgesic effect on

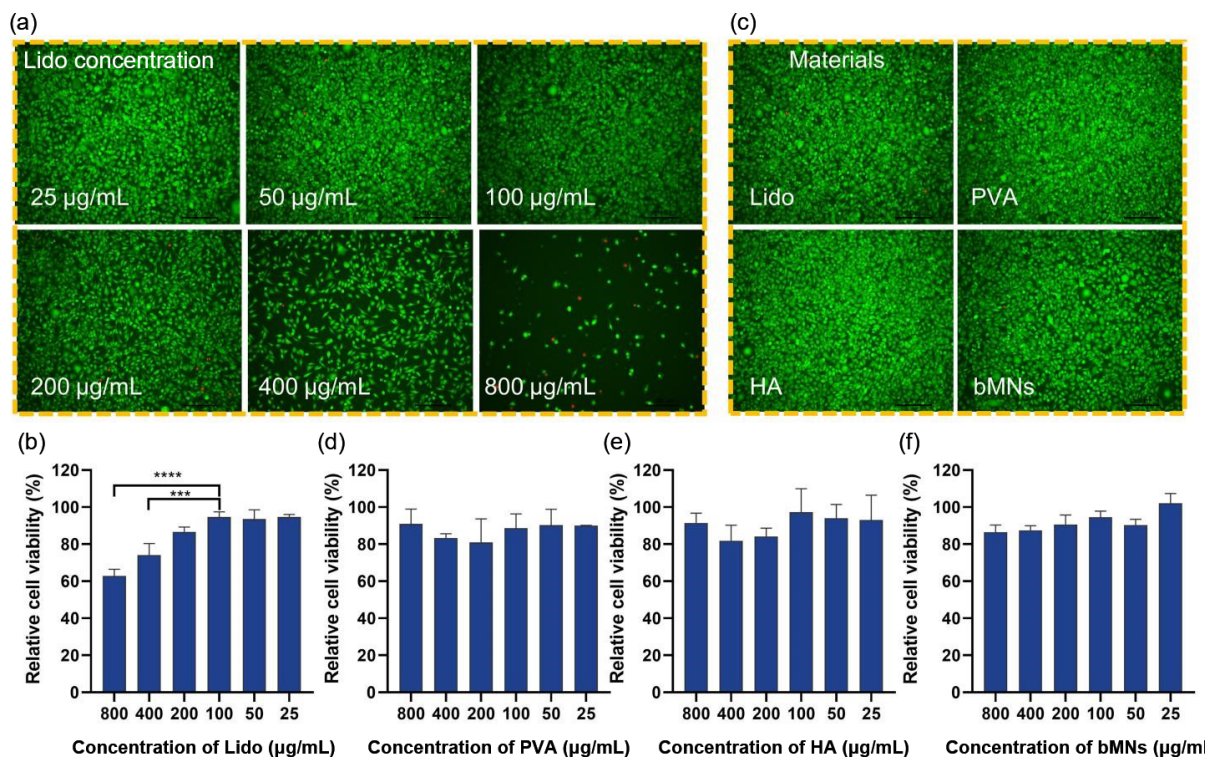


Figure 4 Biosafety assessment. (a) Fluorescence images of L929 cells incubated with various concentrations of Lido. (b) Relative viability of L929 cells incubated with various concentrations of drug (Lido). (c) Fluorescence images of L929 cells incubated with Lido, PVA, HA, and Lido/HA bMNs. (d)–(f) Relative viability of L929 cells incubated with various concentrations of PVA, HA, and Lido/HA bMNs.

mechanical pain. The PWT of Lido/HA bMNP group was significantly increased at 15, 30, 45, and 60 min of post-administration compared to blank, HA bMNP, and Lido HP group. The observed analgesic effect lasted for up to 1 h and reached a maximal effect at 30 min post-Lido/HA bMNP application, as indicated by an increase in the mechanical PWT from 50.2% to 122.9% of preoperative threshold on mechanical pain. Compared with Lido HP, Lido/HA bMNP could directly release more drugs into the skin, which could significantly reduce mechanical allodynia of surgery. Therefore, Lido/HA bMNP could be applied for local analgesia in the field of microplastic surgery.

3 Conclusions

In summary, we designed Lido/HA bMNP encapsulating the precise dose of Lido. The MNs effectively penetrate the skin and fall off under shear after patch administration, and quickly release encapsulated Lido within 15 s for sustained pain relief about 1 h. The Lido/HA bMNP has advantages such as convenient application, rapid onset, high biosafety, and effective analgesic effect. This minimally invasive local analgesia provides convenience and practicality for medical cosmetic surgery, and also brings hope for beauty lovers to reduce and relieve the pain caused by related invasive cosmetic surgery with great clinical significance and practical value.

4 Methods

4.1 Fabrication of Lido/HA bMNP

PDMS (Sylgard 184) was purchased from Dow Corning (Midland, USA). HA ($M_w = 20,000\text{--}400,000$ Da) was purchased from Sigma-Aldrich (MO, USA). Cell counting kits (CCK-8) were obtained from Beijing Solarbio Science & Technology Co., Ltd. (Beijing, China). Lido was purchased from Macklin (Shanghai, China). Male SD rat and BALB/c mice were purchased from the Institute of Laboratory Animal Sciences (Beijing, China)

The Lido/HA matrix material was prepared by adding 1 g of HA ($M_w = 200,000\text{--}300,000$) powder to 10 mL of deionized (DI) water, stirring at 40 °C for 2 h, and then Lido (0.1, 0.2, 0.3, 0.4, and 0.5 g) was mixed at room temperature for 1 h. PDMS (Sylgard 184) negative micromolds were used to fabricate Lido/HA bMNP according to the previously reported method [35]. The patch was designed as a 10×10 array with a needle spacing of 500 µm. Each MN was conical with the height of 600 µm and the base radius of 300 µm. The MNP was prepared by vacuum forming. 100 µL of Lido hydrochloride solution (1, 5, 10, and 20 mg/mL in DI water) was dropped on the PDMS template, and the drug solution was driven into the template cavity by vacuuming. After 90 min, the excess drug solution was removed, and the drug solution in the holes was dried under a vacuum for 30 min. In order to increase the drug loading capacity of the MNP, the above steps were repeated twice. Then the prepared Lido/HA matrix material was coated on the MN mold and kept under vacuum for 10, 30, and 60 min to further fill the mold cavity. After removing the excess Lido/HA matrix material and continuing to vacuumize (5, 10, and 15 min), and a concave structure was formed in the MN cavity. Finally, a thin layer of 35 wt.% PVA solution was applied on PDMS to form the backing layer of the MNP, a bubble was formed between MN and the backing layer, and the Lido/HA bMNP was obtained by demolding and drying. The morphologies of MNPs were observed using an optical/fluorescence microscope (Olympus SZX7, Japan).

4.2 Mechanical and insertion properties of Lido/HA bMNP

An electric displacement force test bench (ESM301, Mark-10, dynamometer model, USA) was used to determine the mechanical properties and insertion properties of the IMP, as described in our previous work. For the test of mechanical properties, the MNP was placed on a metal fixed station, and the mechanical sensor applied an axial force to press MN at a speed of 1.1 mm/s until a

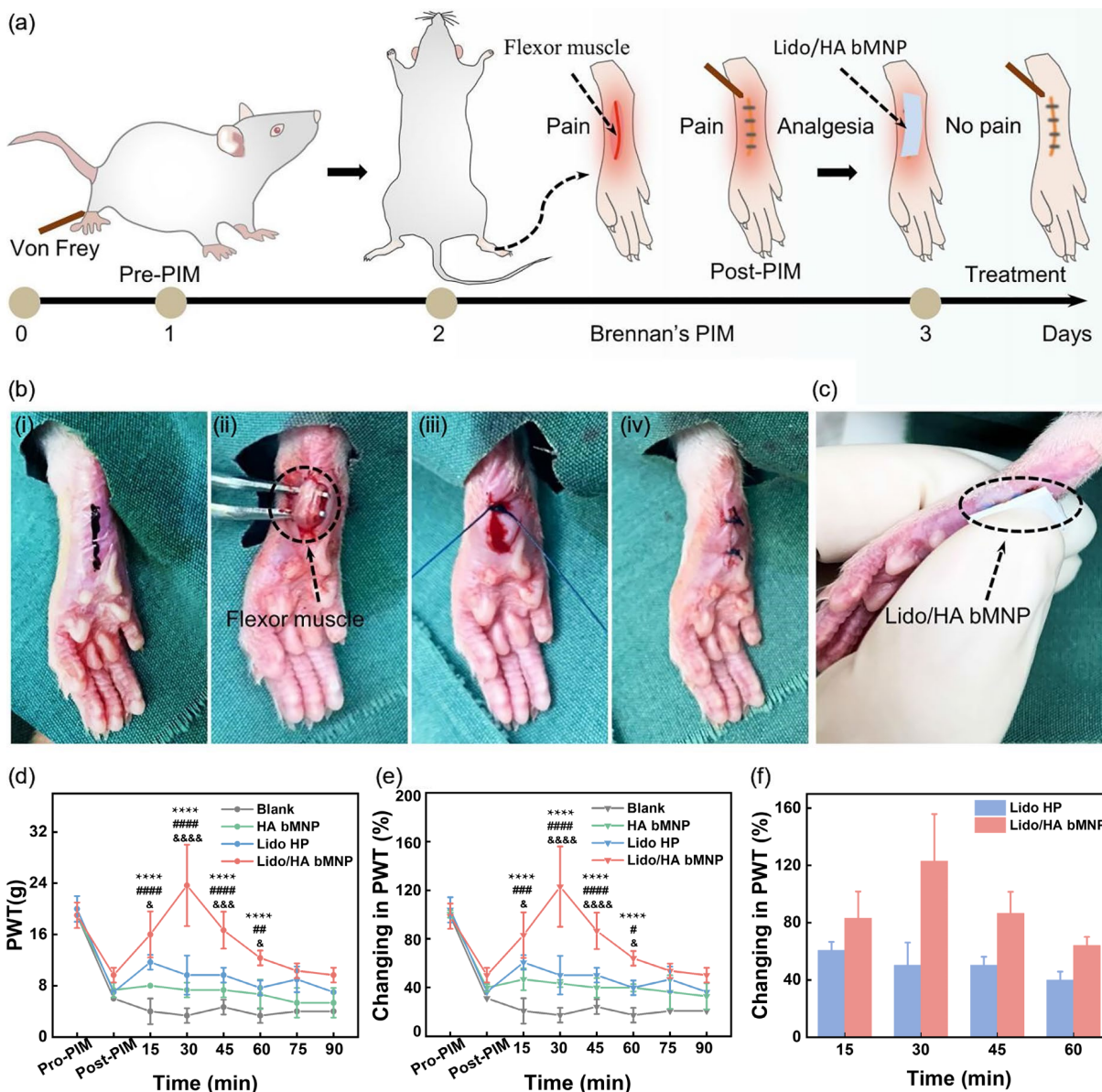


Figure 5 Lido/HA bMNs analgesia *in vivo*. (a) Schematic illustration of Lido/HA bMNP for the analgesia of Brennan's PIM. (b) Pictures of rats constructed with Brennan's plantar incision model. (i) Preparation before an incision. (ii) A 1-cm longitudinal incision was made starting 0.5 cm from the proximal edge of the heel. Flexor muscle was elevated and split by blunt dissection longitudinally. (iii) and (iv) The wound was sutured with two stitches by 4-0 nylon. (c) Picture of rat plantar administration with Lido/HA bMNP. (d) The rats' mechanical pain thresholds to von Frey filaments tested in Blank, HA bMNP, Lido HP, and Lido/HA bMNP groups at different times. (e) Changes in mechanical pain threshold of rats in each group compared to pre-PIM baseline. (f) After treatment with Lido HP and Lido/HA bMNP, the changes of mechanical pain threshold of rats within 15, 30, 45, and 60 min. *, #, & and & indicate the significant differences between groups HA/Lido MNP and blank, HA/Lido MNP and HA MNP, and HA/Lido MNP and HA/Lido HP, respectively.

preset maximum load (20 N) was reached. A function of force and displacement was recorded to evaluate the mechanical properties of MNs. Regarding the insertion test, the fabricated MNP was attached to the mechanical sensor and respectively inserted into biological tissues and artificial membranes with a certain force (10 N). Prior to penetration testing, hair of the back skin was carefully removed using a disposable razor, and the parafilm was folded into an eight-layer sheet (approximately 1 mm thick) to achieve the thickness of human skin. The insertion ability of MNP was determined by evaluating the number of holes in each layer of parafilm and the puncture marks of the mouse skin under a brightfield microscope.

4.3 Drug delivery *in vitro*

The drug loading of Lido of Lido/HA bMNP was quantified by high-performance liquid chromatography (HPLC, Elite 230II, with a P 230II pump and UV 230II detector). Lido/HA bMNP

was soaked in 0.01 M PBS, and the soaking liquid was pretreated with a 1,000 Mw ultrafiltration centrifuge tube to remove HA. Lido concentrations were performed by reversed-phase high performance liquid chromatography at 254 nm, using a C18 column (Supersil ODS2, 5 μm, 4.6 mm × 150 mm). A mixture of 0.1 M KH₂PO₄ buffer and acetonitrile (50:50, v/v) was used as the mobile phase.

4.4 Drug delivery *in vivo*

Animal experiments complied with the guidelines of National Institutes of Health (NIH) and were totally approved by the Institutional Animal Care and Use Committee of the Cancer Institute and Cancer Hospital Chinese Academy of Medical Sciences prior to initiation of studies (ethical approval number: NCC2021A275). To visualize drug release *in vivo*, rhodamine B, as a model drug, was encapsulated in MNP instead of Lido hydrochloride. Six BALB/c mice (6–8 weeks) were treated by

MNP and HP loaded with the same dose of drug, HP as control group. Mice were imaged using an *in vivo* imaging system (IVIS spectrum, PE), and the fluorescence intensity of the administered area was measured to analyze the drug release efficiency *in vivo*.

4.5 Biosafety assessment

L929 fibroblast cells were used to evaluate the toxicity of Lido drug and Lido/HA bMNP matrix materials. Specifically, L929 cells were inoculated in 96-well plates at a density of 1×10^4 cells/well and cultured in cell culture medium (1% penicillin-streptomycin solution, 10% fetal bovine serum, and 89% dulbecco's modified eagle's medium (DMEM)) containing 200 μL , 25, 50, 100, 200, 400, and 800 $\mu\text{g}/\text{mL}$ of Lido, PVA, HA, and bMNP, respectively. Among them, the culture medium of Lido/HA bMNs was prepared by dissolving 0.8 mg of bubble MNs in 1, 2, 4, 8, 16, and 32 mL of DMEM cell culture medium. After the cells were incubated in a constant temperature and humidity chamber (37 °C and 5% CO_2) for 24 h, the Calcein-AM/PI kit was used to perform double staining and labeling of live and dead cells. Cell fluorescence images were captured by confocal fluorescence microscopy (Leica SP8). CCK-8 was used to assess cell viability, and the absorbance of each well was measured by a microplate reader (BioRad iMark) at a wavelength of 450 nm.

4.6 Plantar incision model

The Brennan's plantar incision model was created in male SD rats (200 \pm 10 g) to evaluate the analgesic effect of MNP. Anesthesia was induced and maintained with sevoflurane in oxygen and spontaneous respiration. The surgical incision was marked with a black marker pen on the left hind paw. The hind paw was placed through a hole in a sterile cloth and aseptically treated with 10% povidone-iodine solution. At the starting point from the 0.5 cm of the proximal edge of the heel, a 1-cm longitudinal incision was made with a number 11 blade, and the skin and fascia were cut open to expose the toe muscle. The flexor digitorum brevis muscle was raised and split longitudinally by blunt dissection, and the muscle origin and insertion were kept intact. After hemostasis, the wound was sutured with two stitches by 4-0 nylon on FS-2 needle. After the operation, the rats were put back into their original cage and recovered from anesthesia for about 15 min.

4.7 Lido/HA bMNs analgesia *in vivo*

SD rats created with the Brennan's plantar incision model were randomly divided into 4 groups and treated in four ways: blank (no treatment), Lido HP, HA bMNP (without drugs), and Lido/HA bMNP. The analgesic effect of the patch was assessed by measuring the mechanical PWT and the hind-paw licking latency. The von Frey test was used to measure the mechanical nociceptive threshold in rats. Individual rats were placed in separate plastic chambers (15 cm \times 15 cm \times 30 cm) with a mental mesh at the bottom, which was suspended on a bracket. Restraints on rats should be minimized so as not to affect behavior tests. After 30 min of adaptation, the PWT was tested by means of von Frey filaments (ZS-Vofry, ZS Dichuang, China) with bending forces of 2, 4, 6, 8, 10, 15, 26, and 60 g applied by turn from beneath the cage through the mesh floor to the plantar skin of planned surgical area. Each time the von Frey hair was kept bent for 2 to 3 s, and each filament was applied 3 times with a 5 s interval. If the paw withdrawal happened 2 out of 3 times, this force was considered as the mechanical PWT. If there was still no response at the bending force of 60 g, then 60 g was assigned as the cutoff value. The mechanical measurements of rats were expressed as the PWT at the corresponding time and a percentage of the normal nociception measured before PIM surgery, respectively.

Acknowledgements

This work was financially supported by the National Natural Science Foundation of China (Nos. 61875015 and T2125003), the Strategic Priority Research Program of the Chinese Academy of Sciences (No. XDA16021101), and Beijing Natural Science Foundation (Nos. JQ20038, L212010, and L212046).

References

- [1] Abdelmoniem, S. A.; Mahmoud, S. A. Comparative evaluation of passive, active, and passive-active distraction techniques on pain perception during local anesthesia administration in children. *J. Adv. Res.* **2016**, *7*, 551–556.
- [2] Templeton, T. W.; Sommerfield, D.; Hii, J.; Sommerfield, A.; Matava, C. T.; Von Ungern-Sternberg, B. S. Risk assessment and optimization strategies to reduce perioperative respiratory adverse events in Pediatric Anesthesia—Part 2: Anesthesia-related risk and treatment options. *Paediatr. Anaesth.* **2022**, *32*, 217–227.
- [3] Jayakumar, A.; Jose, V. K.; Lee, J. M. Hydrogels for medical and environmental applications. *Small Methods* **2020**, *4*, 1900735.
- [4] Weldon, C.; Ji, T. J.; Nguyen, M. T.; Rwei, A.; Wang, W. P.; Hao, Y.; Zhao, C.; Mehta, M.; Wang, B. Y.; Tsui, J. et al. Nanoscale bupivacaine formulations to enhance the duration and safety of intravenous regional anesthesia. *ACS Nano* **2019**, *13*, 18–25.
- [5] Rwei, A. Y.; Sherburne, R. T.; Zurakowski, D.; Wang, B. B. S.; Kohane, D. S. Prolonged duration local anesthesia using liposomal bupivacaine combined with liposomal dexamethasone and dexmedetomidine. *Anesth. Analg.* **2018**, *126*, 1170–1175.
- [6] Santamaria, C. M.; Woodruff, A.; Yang, R.; Kohane, D. S. Drug delivery systems for prolonged duration local anesthesia. *Mater. Today* **2017**, *20*, 22–31.
- [7] Albright, G. A. Cardiac arrest following regional anesthesia with etidocaine or bupivacaine. *Anesthesiology* **1979**, *51*, 285–287.
- [8] Yamashita, A.; Matsumoto, M.; Matsumoto, S.; Itoh, M.; Kawai, K.; Sakabe, T. A comparison of the neurotoxic effects on the spinal cord of tetracaine, lidocaine, bupivacaine, and ropivacaine administered intrathecally in rabbits. *Anesth. Analg.* **2003**, *97*, 512–519.
- [9] Katz, N. P.; Shapiro, D. E.; Herrmann, T. E.; Kost, J.; Custer, L. M. Rapid onset of cutaneous anesthesia with EMLA cream after pretreatment with a new ultrasound-emitting device. *Anesth. Analg.* **2004**, *98*, 371–376.
- [10] Lei, Q.; He, D. F.; Ding, L. P.; Kong, F. H.; He, P. Y.; Huang, J. D.; Guo, J. M.; Brinker, C. J.; Luo, G. X.; Zhu, W. et al. Microneedle patches integrated with biomimetic melanin nanoparticles for simultaneous skin tumor photothermal therapy and wound healing. *Adv. Funct. Mater.* **2022**, 2113269.
- [11] Yang, Y.; Xu, L. L.; Jiang, D. J.; Chen, B. Z.; Luo, R. Z.; Liu, Z.; Qu, X. C.; Wang, C.; Shan, Y. Z.; Cui, Y. et al. Self-powered controllable transdermal drug delivery system. *Adv. Funct. Mater.* **2021**, *31*, 2104092.
- [12] Zhou, Z. Z.; Pang, J. H.; Wu, X. J.; Wu, W.; Chen, X. G.; Kong, M. Reverse immune suppressive microenvironment in tumor draining lymph nodes to enhance anti-PD1 immunotherapy via nanovaccine complexed microneedle. *Nano Res.* **2020**, *13*, 1509–1518.
- [13] Wan, T.; Pan, Q.; Ping, Y. Microneedle-assisted genome editing: A transdermal strategy of targeting *NLRP3* by CRISPR-Cas9 for synergistic therapy of inflammatory skin disorders. *Sci. Adv.* **2021**, *7*, eabe2888.
- [14] Kim, Y. C.; Park, J. H.; Prausnitz, M. R. Microneedles for drug and vaccine delivery. *Adv. Drug Deliv. Rev.* **2012**, *64*, 1547–1568.
- [15] Sullivan, S. P.; Koutsonanos, D. G.; Del Pilar Martin, M.; Lee, J. W.; Zarnitsyn, V.; Choi, S. O.; Murthy, N.; Compans, R. W.; Skountzou, I.; Prausnitz, M. R. Dissolving polymer microneedle patches for influenza vaccination. *Nat. Med.* **2010**, *16*, 915–920.
- [16] Xu, L. L.; Yang, Y.; Mao, Y. K.; Li, Z. Self-powerability in electrical stimulation drug delivery system. *Adv. Mater. Technol.* **2022**, *7*, 2100055.
- [17] Luo, F. Q.; Chen, G. J.; Xu, W.; Zhou, D. J.; Li, J. X.; Huang, Y. C.; Lin, R.; Gu, Z.; Du, J. Z. Microneedle-array patch with pH-sensitive

- formulation for glucose-responsive insulin delivery. *Nano Res.* **2021**, *14*, 2689–2696.
- [18] Jamaledin, R.; Yiu, C. K. Y.; Zare, E. N.; Niu, L. N.; Vecchione, R.; Chen, G. J.; Gu, Z.; Tay, F. R.; Makvandi, P. Advances in antimicrobial microneedle patches for combating infections. *Adv. Mater.* **2020**, *32*, 2002129.
- [19] Yu, J. C.; Wang, J. Q.; Zhang, Y. Q.; Chen, G. J.; Mao, W. W.; Ye, Y. Q.; Kahkoska, A. R.; Buse, J. B.; Langer, R.; Gu, Z. Glucose-responsive insulin patch for the regulation of blood glucose in mice and minipigs. *Nat. Biomed. Eng.* **2020**, *4*, 499–506.
- [20] Li, X. L.; Huang, X. S.; Mo, J. S.; Wang, H.; Huang, Q. Q.; Yang, C.; Zhang, T.; Chen, H. J.; Hang, T.; Liu, F. M. et al. A fully integrated closed-loop system based on mesoporous microneedles-iontophoresis for diabetes treatment. *Adv. Sci.* **2021**, *8*, 2100827.
- [21] Donnelly, R. F.; Singh, T. R. R.; Garland, M. J.; Migalska, K.; Majithiya, R.; McCrudden, C. M.; Kole, P. L.; Mahmood, T. M. T.; McCarthy, H. O.; Woolfson, A. D. Hydrogel-forming microneedle arrays for enhanced transdermal drug delivery. *Adv. Funct. Mater.* **2012**, *22*, 4879–4890.
- [22] Jin, X.; Zhu, D. D.; Chen, B. Z.; Ashfaq, M.; Guo, X. D. Insulin delivery systems combined with microneedle technology. *Adv. Drug Deliv. Rev.* **2018**, *127*, 119–137.
- [23] Than, A.; Liang, K.; Xu, S. H.; Sun, L.; Duan, H. W.; Xi, F. N.; Xu, C. J.; Chen, P. Transdermal delivery of anti-obesity compounds to subcutaneous adipose tissue with polymeric microneedle patches. *Small Methods* **2017**, *1*, 1700269.
- [24] Xie, X.; Pascual, C.; Lieu, C.; Oh, S.; Wang, J.; Zou, B. D.; Xie, J. L.; Li, Z. H.; Xie, J.; Yeomans, D. C. et al. Analgesic microneedle patch for neuropathic pain therapy. *ACS Nano* **2017**, *11*, 395–406.
- [25] Zhao, Z. Q.; Zhang, B. L.; Chu, H. Q.; Liang, L.; Chen, B. Z.; Zheng, H.; Guo, X. D. A high-dosage microneedle for programmable lidocaine delivery and enhanced local long-lasting analgesia. *Mater. Sci. Eng. C* **2021**, 112620.
- [26] Yin, M. T.; Xiao, L.; Liu, Q. C.; Kwon, S. Y.; Zhang, Y.; Sharma, P. R.; Jin, L.; Li, X. D.; Xu, B. X. 3D printed microheater sensor-integrated, drug-encapsulated microneedle patch system for pain management. *Adv. Healthc. Mater.* **2019**, *8*, 1901170.
- [27] Li, Q. Y.; Zhang, J. N.; Chen, B. Z.; Wang, Q. L.; Guo, X. D. A solid polymer microneedle patch pretreatment enhances the permeation of drug molecules into the skin. *RSC Adv.* **2017**, *7*, 15408–15415.
- [28] Waghule, T.; Singhvi, G.; Dubey, S. K.; Pandey, M. M.; Gupta, G.; Singh, M.; Dua, K. Microneedles: A smart approach and increasing potential for transdermal drug delivery system. *Biomed. Pharmacother.* **2019**, *109*, 1249–1258.
- [29] Al Sulaiman, D.; Chang, J. Y. H.; Bennett, N. R.; Topouzi, H.; Higgins, C. A.; Irvine, D. J.; Ladame, S. Hydrogel-coated microneedle arrays for minimally invasive sampling and sensing of specific circulating nucleic acids from skin interstitial fluid. *ACS Nano* **2019**, *13*, 9620–9628.
- [30] Chang, H.; Zheng, M. J.; Chew, S. W. T.; Xu, C. J. Advances in the formulations of microneedles for manifold biomedical applications. *Adv. Mater. Technol.* **2020**, *5*, 1900552.
- [31] Yang, G.; Chen, Q.; Wen, D.; Chen, Z. W.; Wang, J. Q.; Chen, G. J.; Wang, Z. J.; Zhang, X. D.; Zhang, Y. Q.; Hu, Q. Y. et al. A therapeutic microneedle patch made from hair-derived keratin for promoting hair regrowth. *ACS Nano* **2019**, *13*, 4354–4360.
- [32] Sun, Y.; Chen, M. L.; Yang, D.; Qin, W. B.; Quan, G. L.; Wu, C. B.; Pan, X. Self-assembly nanomicelle-microneedle patches with enhanced tumor penetration for superior chemo-photothermal therapy. *Nano Res.* **2022**, *15*, 2335–2346.
- [33] Wang, C. Y.; Jiang, X.; Zeng, Y. N.; Terry, R. N.; Li, W. Rapidly separable microneedle patches for controlled release of therapeutics for long-acting therapies. *Med. Drug Discov.* **2022**, *13*, 100118.
- [34] Zhan, H. H.; Ma, F. S.; Huang, Y. C.; Zhang, J.; Jiang, X. Y.; Qian, Y. C. Application of composite dissolving microneedles with high drug loading ratio for rapid local anesthesia. *Eur. J. Pharm. Sci.* **2018**, *121*, 330–337.
- [35] Wang, Q. L.; Zhu, D. D.; Liu, X. B.; Chen, B. Z.; Guo, X. D. Microneedles with controlled bubble sizes and drug distributions for efficient transdermal drug delivery. *Sci. Rep.* **2016**, *6*, 38755.
- [36] Suárez-Hernández, L. A.; Camacho-Ruiz, R. M.; Arriola-Guevara, E.; Padilla-Camberos, E.; Kirchmayr, M. R.; Corona-González, R. I.; Guatemala-Morales, G. M. Validation of an analytical method for the simultaneous determination of hyaluronic acid concentration and molecular weight by size-exclusion chromatography. *Molecules* **2021**, *26*, 5360.
- [37] Gotoh, S.; Onaya, J. I.; Abe, M.; Miyazaki, K.; Hamai, A.; Horie, K.; Tokuyasu, K. Effects of the molecular weight of hyaluronic acid and its action mechanisms on experimental joint pain in rats. *Ann. Rheum. Dis.* **1993**, *52*, 817–822.
- [38] Zhang, L. Q.; Zhang, X. P.; Hao, Y. Y.; Zhang, B. L.; Guo, X. D. Codelivery of hydrophilic and hydrophobic drugs in a microneedle patch for the treatment of skin pigmentation. *J. Ind. Eng. Chem.* **2020**, *88*, 241–250.
- [39] Pan, C. Y.; Li, X. C.; Sun, J.; Li, Z.; Zhang, L.; Qian, W. P.; Wang, P. M.; Dong, J. A multiplexed SERS-active microneedle for simultaneous redox potential and pH measurements in rat joints. *ACS Appl. Bio Mater.* **2019**, *2*, 2102–2108.
- [40] Chen, B. Z.; Zhang, L. Q.; Xia, Y. Y.; Zhang, X. P.; Guo, X. D. A basal-bolus insulin regimen integrated microneedle patch for intraday postprandial glucose control. *Sci. Adv.* **2020**, *6*, eaba7260.
- [41] Liu, X. M.; Yan, J. Y.; Wu, X. P.; Wu, X.; Zhang, Y. J.; Li, B. Biosafety evaluation of Li₂Si₂O₅ whisker-reinforced glass-ceramics. *Biomed. Mater.* **2022**, *17*, 025011.
- [42] Yu, X.; Ren, X. L.; Wang, M.; Wang, K.; Zhang, D. Q. Evaluation of biosafety/biocompatibility of calixpyridinium on different cell lines. *J. Incl. Phenom. Macrocycl. Chem.* **2021**, *99*, 109–115.
- [43] Brennan, T. J.; Vandermeulen, E. P.; Gebhart, G. F. Characterization of a rat model of incisional pain. *Pain* **1996**, *64*, 493–502.